Noname manuscript No.
(will be inserted by the editor)

Sensitively photoelastic biocompatible gelatin spheres for investigation of locomotion in granular media

Seyed Amir Mirbagheri · Ericson Ceniceros · Mehdi Jabbarzadeh · Zephyr McCormick · Henry Chien Fu

Received: date / Accepted: date

Abstract We present a method for measuring forces in granular media experiments using photoelastic gelatin spheres, which is applicable for investigating the forces generated by organisms moving through noncohesive granular materials. We describe how to fabricate gelatin spheres with appropriate characteristics for high-sensitivity photoelastic measurements. We present a calibration methodology to relate photoelastic signal to force applied to the spheres, and evaluate the photoelastic performance of gelatin spheres as a function of gelatin concentration. The spheres can be used across a range of salinities, allowing investigation of freshwater and marine organisms. We show that photoelastic gelatin spheres can detect forces as small as 1 μN, and quantitatively measure forces with up to 60 μN precision. We provide a proof-of-principle experiment in which the forces exerted by an earthworm in a granular environment are measured.

Keywords Photoelasticity · Force measurement · Granular materials · Biolocomotion · Burrowing;

1 Introduction

Many animals burrow into substrates like sand, soil and muddy sediments. Muddy sediments cover the vast majority of the earth's surface if areas underwater are included [15]. Through bioturbation, burrowing animals can have great environmental and ecological consequences, including of agricultural relevance for species such as earthworms (*Lumbricus terrestis*). Burrowing occurs across a range of scales, from nematode worms ($\sim$ 1 mm long, $\sim$ 100 μm diameter), larger marine and terrestrial worms ($\sim$ 10 cm long, 1 cm diameter), to vertebrates such as sandfish lizards and eels ($\sim$ 10 cm long) and moles ($\sim$ 20 cm long). However, understanding the mechanics of burrowing is difficult since underground motion is hard to observe and the mechanics of soils and sediments is complex, as they are heterogeneous substrates composed of particulates and organic material.

It has been shown that depending on the mechanical properties of the medium, burrowing can proceed by a number of different mechanisms. In elastic cohesive sediments, worms extend burrows by propagating cracks[1, 3, 15], often by using anterior body segments[1], a pharynx[3], or proboscis[15] which can expand and generate stresses. In contrast, noncohesive media can undergo (possibly large) rearrangement of particles as organisms move through them. In noncohesive media, sandfish lizards[14] use undulatory body kinematics and razor clams contract valves[20] to fluidize their granular surroundings to enable propulsion. Undulatory motions can also be effective when granular media have a more solid-like response, such as in the case for the polychaete *Armandia brevis*[4], or at microscales, such as for the nematode *C. elegans*[11, 12].

Our understanding of burrowing in cohesive sediments, in which burrows propagate by crack fracture, has been advanced by the development of transparent photoelastic model substrates (gelatin) which allow the simultaneous observation of burrowing kinematics and visualization and quantification of forces and stresses in the substrate during burrowing. In this paper we describe the development of an analogous model substrate for noncohesive granular media, which will allow

Seyed Amir Mirbagheri, Ericson Ceniceros, Mehdi Jabbarzadeh, and Henry Chien Fu
Department of Mechanical Engineering, University of Nevada Reno, Reno, NV 89557 USA. E-mail: hfu@unr.edu

Zephyr McCormick
Department of Physics, University of Nevada Reno, Reno, NV 89557 USA.

the visualization and quantification of burrowing forces in noncohesive particulate media.

Observations of burrowing and locomotion in granular models[12, 11, 20, 14] have revealed much about the kinematics of burrowing, but have yielded less clear-cut information about the forces exerted during burrowing. Previously, forces in granular media have been investigated through the photoelastic effect using plastic disks[13]. These photoelastic experiments require a two-dimensional geometry with the disks confined between two transparent plates. This type of experiment can quantify forces in centiNewton[19] or milliNewton [5]ranges. In our study, we use gelatin as a photoelastic substrate. As a bulk solid in planar geometries, gelatin has previously been used as a model cohesive medium (as described above)[3], as well as to measure forces during insect locomotion[6]. Due to its low elastic modulus, gelatin is an extremely sensitive photoelastic substrate, and has been used to detect forces as low as 98 nN[8].

While burrowing, the forces exerted by larger organisms such as sandfish, clams, or eels can be as large as 1-10 N[14, 20, 9] but may be significantly smaller for earthworms (0.1-1 N)[17], marine worms (0.01 N)[3] and nematodes such as C elegans (10^{-6} N)[7, 2]. While plastic photoelastic disks are sensitive enough to measure the maximum forces of all but the smallest of these organisms, the sensitivity afforded by gelatin spheres allows greater resolution of the nonmaximal dynamical forces during all phases of locomotion. In addition, forces in noncohesive environments are likely to be smaller than in cohesive media since less force may be required to rearrange grains rather than fracture cohesive materials. Furthermore, in 2-D geometries, as the thickness of plastic disks increases and approaches the disk diameter, it becomes more difficult to prevent the disks from flipping during experiments (Private communication, Abe Clark, Duke University and Vishay technical representative). In a 2-D environment, this makes it difficult to use disks to study burrowing, since the grain sizes in most substrates are typically the same size or smaller than the width of burrowing worms, and thin plastic disks may not accommodate the width of organisms. Gelatin, on the other hand, has the capability to measure forces down to scales appropriate for the smallest nematodes, and can be fabricated in a variety of geometries.

Thus, to investigate forces in burrowing locomotion of different organisms, we fabricated gelatin photoelastic spheres that can form a granular media. Like previous researchers, we used gelatin because it is twice as sensitive as other photoelastic materials[8], nontoxic, and biocompatible. We show how the photoelastic signal can be calibrated to yield quantitative measurement of applied force. Our experiments indicate that the force detection threshold of our spheres is $< 1\,\mu$m and forces can be quantified within an uncertainty of $\sim 60\,\mu$N, the latter of which is two orders smaller than possible with the plastic disks used in previous studies of granular media. These characteristics make them appropriate for investigation of animal force production while burrowing in noncohesive granular sands. We provide a proof-of-principle by observing earthworm locomotion through a granular medium composed of our gelatin spheres.

2 Methods

Polariscope Design Photoelastic detection of stress is a well-developed experimental technique for stress and force visualization. If light is passed through two plane polarizing filters with polarization axes oriented perpendicularly, there is no transmission. A photoelastic material has a local birefringence which is linearly related to the strain field. If an unstressed photoelastic material is placed between the polarizers, there is still no transmission since the material is not birefringent. However, a stressed photoelastic material is birefringent, hence rotates the light polarization if placed between the filters, and so light is transmitted through the second filter. The resulting illumination pattern can be correlated to the strain field and ultimately stresses and forces acting on the photoelastic material[10].

Our experiments were conducted with the linear polariscope shown in (Fig. 1) consisting of a light source, two crossed linear polarizers (Edmund Optics Polarizing 0.75mm Thickness Laminated Film NT86-189), and a test section between the polarizers. The light source consisted of two 4 Watt green LEDs (Osram Sylvania, PAR 16 LED Bulbs), which have an emission band centered at 525 nm. The lights were reflected off a diffusing mirror (made from crumpled aluminum foil) and passed through two sheets of diffusing film to achieve an adequate level of diffusion before reaching the test section of the polariscope. A DSLR camera (Canon EOS T3i) was used for image capture. Skirts of opaque black cloth were used to eliminate undesired light from entering the camera sensor.

Gelatin Sphere Fabrication We developed a fabrication process which yields a large number of gelatin spheres with uniform properties at low cost. Gelatin solution was mixed in concentrations ranging from 6% to 14% (mass %) in a beaker. The beaker was covered to minimize evaporation then stirred while heated to 60° C, and held at that temperature for approximately 15 minutes. A graduated cylinder was filled with toluene and

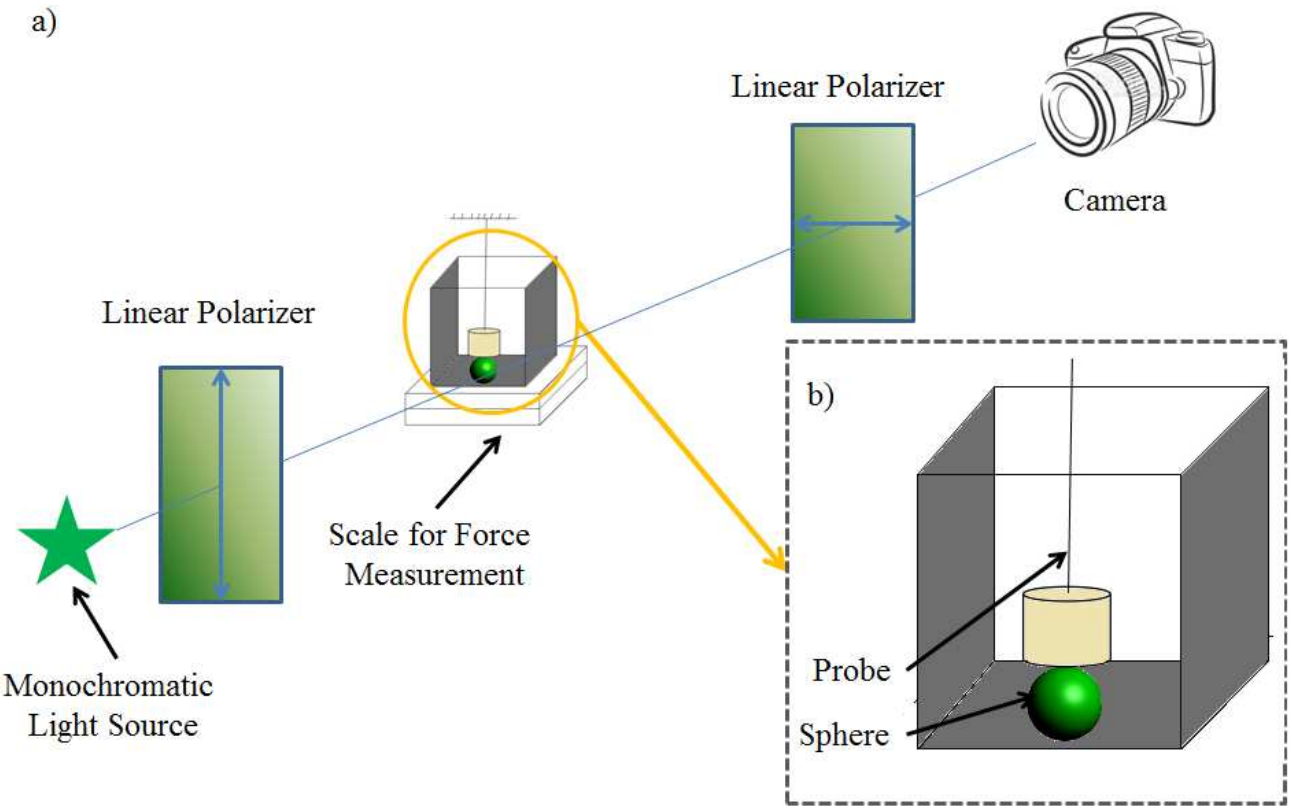

Fig. 1 a) Schematic of polariscope set up to perform sphere calibrations b) Test vessel filled with NaCl solution to eliminate lensing from gelatin spheres. Spheres were placed inside the vessel and rested on the bottom during calibration.

immersed in an ice bath. Individual droplets were made by dripping liquid gelatin from a syringe into the toluene coolant at a rate of approximately 1 drop per second with the dispensing tip half an inch from the surface of the toluene. The surface tension at the toluene-gelatin interface formed the droplets into spheres, which cooled and set as they sank to the bottom of the graduated cylinder. The size of gelatin spheres could be controlled by changing the size and material of the dispensing tip. Different dispensing tips allowed the controlled fabrication of spheres between 2mm to 6.5mm. The toluene had to be below 8°C to solidify the spheres enough to hold their shape while sitting at the bottom. The spheres were then removed from the cylinder and placed in an open petri dish to allow the remaining toluene to evaporate. Once dry, the spheres were placed in a storage solution of 0 to 1 M NaCl. NaCl solution prevents the spheres from breaking apart over long periods of time. At 0 M, the spheres must be used within a few days or they dissolve; above 0.14 M they can be stored for weeks.

Gelatin is prone to fluctuations in hydration which leads to residual stresses that affect photoelastic signal[8]. Previous research groups working with bulk (nonspherical) gelatin substrates overcame the hydration problem by forming the gelatin in molds and covering it with wet cloth. Glycerol has also been added to gelatin as a humectant. These previous researchers solved the residual stress problem by annealing the gelatin while still in the molds, by heating it to just below its melting point and holding it there for 30-45 minutes[6, 8]. We did not have success with these procedures. Our technique was sensitive enough to detect residual stress from even slight dehydration, and the amount of time required to form spheres in the process described above was too long to prevent such slight dehydration. We also tested several batches of gelatin with varying concentrations of glycerol additives, but found that it decreased the sensitivity of gelatin spheres. Finally, due to the spherical geometries, there was no rigid mold to contain the gelatin during annealing, which results in the spheres deforming or breaking apart completely when heated to near melting point.

Instead, we removed residual stress by annealing the spheres at elevated temperatures which were still far below the melting point over long periods of time in an incubator. For example, spheres made of up to 12% gelatin incubated at 20°C for 48 hours showed no residual stress. For higher gelatin concentrations increased temperatures are required; *e.g.* for spheres made of 14%

gelatin incubation temperatures of 23°C were needed to remove residual stress.

Force Measurement and Signal Calibration We performed calibration experiments to establish a direct correlation between the force applied to a sphere and the amount of birefringent signal it produced. To eliminate lensing effects, a gelatin sphere (which has an index of refraction close to that of water) was immersed in NaCl storage solution held in a calibration vessel (Fig. 1b machined out of one piece of polyoxymethylene with two opposing parallel walls made from stress free glass. The glass was bonded to the plastic container with nonbirefringent adhesive (Momentive RTV108 Silicone Rubber adhesive.) A vertical force was exerted on the sphere by a probe extending into the vessel.

Forces applied to spheres in the calibration process were measured with a laboratory balance with 0.1 mg sensitivity (Sartorius CP64, Fig. 1a). The balance was placed on a high precision jack (Thorlab L490) capable of being raised and lowered in increments of 10 μm as measured by a height gauge. The bottom of the jack was rigidly attached to the bottom of the polariscope frame. The probe was secured to the top of the polariscope frame and positioned in the container over a gelatin sphere. Force was applied by raising the jack and balance assembly to compress the sphere against the probe tip and the resulting reaction force was read from the balance (Fig. 1a).

A full calibration run proceeded as follows: First, a sphere was placed in the test container, which was filled with NaCl storage solution and placed on the balance. The probe was lowered into the container and secured to the top of the polariscope frame. The first picture was taken with the probe slightly above the sphere and at the same time the balance and height gauge were zeroed. This served as a reference state that all other photos were compared to. The jack was raised slightly, another photo was taken, and the balance and height gauge readings were recorded. This was repeated until the maximum desired force was reached. The sphere was then unloaded in similar increments and the same data was recorded. The resulting image sequence showed a photoelastic signal that increased in intensity with increasing load (Fig. 2).

Systematic Errors in Force Measurements The sphere was immersed in water while being tested to eliminate the lensing effect of the spherical geometry, since the index of refraction of the fabricated spheres were very close to that of water. In water, we observed that the spheres did not adhere to one another and were very slippery, implying that forces on the spheres are dominated by normal components. This approach introduced three sources of error: evaporation of water from the container, the buoyancy force from the probe displacing water as it was lowered in to the container, and surface tension forces from the meniscus around the probe.

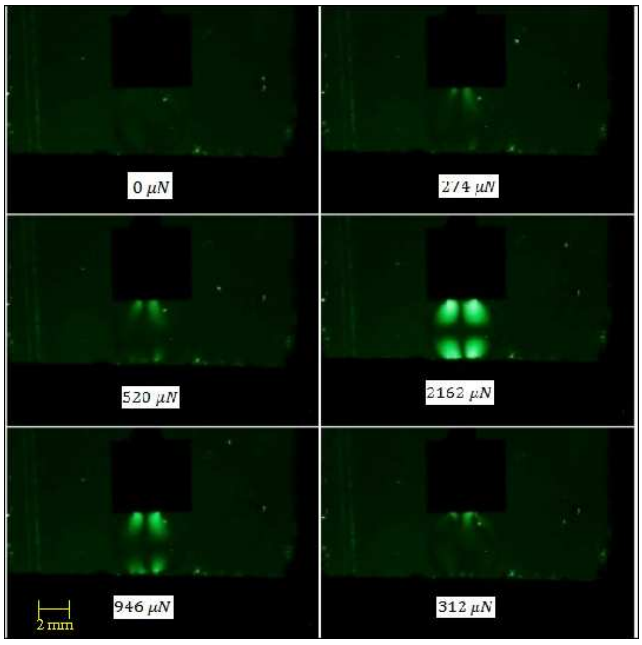

Fig. 2 Example of a typical compression/decompression cycle for photoelastic gelatin sphere calibration. All figures have the same scale.

To account for evaporation, we found an average rate of evaporation during each experiment by measuring the evaporation from the container over a period of minutes before and after each experiment. The rate of evaporation changed day to day, but never varied more than 5% over the course of an experiment. Measured rates of evaporation depended on environmental temperature and humidity and ranged from 0.2 to 0.4 μN/s. We corrected for weight loss due to evaporation by using time stamps on each photo to find the elapsed time, and adding the product of elapsed time and average evaporation rate to the indicated weight on the scale.

The buoyancy force was calculated by finding the quantity of water displaced by the probe as it was immersed in the test container. Our results show that when using a thin probe, the buoyancy force has an insignificant effect on force measurements. With the probe used for the calibration, the maximum error in force measurements caused by the buoyancy force was 2 μN, so we ignored it for the calibration.

Surface tension forces were the most difficult to account for because they were not constant or predictable. An approximate surface tension force due to the menis-

cus can be calculated as $F_\sigma = \gamma LCos(\alpha) = 0.397\mu$N, where γ=0.001 N/m is surface tension of water, L is the circumference of the probe at the surface, and α is contact angle between water. For a maximal estimate, we assume that $\alpha = 0°$. However, based on our observations and measurements, this was not a quantitative estimate, since the meniscus shape varied as the probe traveled into and out of the fluid. Small vibrations in the table and different directions of probe travel caused unpredictable behavior of the meniscus. It was found that the surface tension error caused a random noise in the data that was most prevalent when inserting the probe into the water and less prevalent pulling it out. To reduce the surface tension force we used a thin probe to reduce the contact length. As discussed above, the thin probe had the added benefit of reducing the buoyancy force.

Image Analysis Images captured during experimentation were analyzed using MatLab. For example, in (Fig. 3), hot areas correspond to regions of high green values and higher signal intensity. Photoelastic response was determined by calculating the pixel-averaged green intensity over the projected area of each sphere. Using the pixel-averaged intensity made it possible to compare images with different diameters and sphere shapes as the sphere was compressed. We correlated the applied force on the sphere to the change in pixel-averaged intensity,

$$\Delta I_{avg} = \frac{I}{N} - \frac{I_0}{N_0}, \quad (1)$$

where I is the total intensity of projected area, N is the number of pixels of projected area, and the subscript 0 refers to the image of the unstressed sphere, considered as a reference. Comparison with the reference image eliminates noise resulting from vessel imperfections and scattering from contaminants in the NaCl solution.

We tested a variety of image analysis algorithms to identify the boundary of the projected area of the sphere. We compared algorithms that fit the boundary to a circle or rectangle, as well as a boundary manually selected by the user. Representative boundaries are shown in Fig. 3b. Although different boundary-determination algorithms yielded different quantitative values for the pixel-averaged intensity of a sphere, all yielded the same trends and were equally suitable for calibration provided a consistent boundary determination method was used.

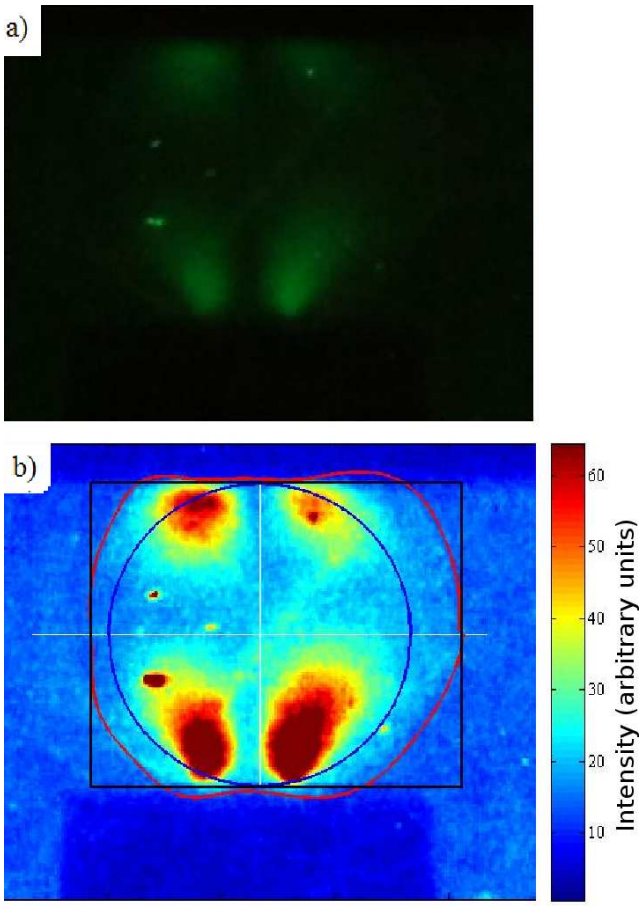

Fig. 3 a) Image of loaded sphere. b) A pseudocolor map of intensity on the same sphere. Lines indicate different boundaries for the averaging area tested by image processing algorithm (see text; black and blue were generated by image processing algorithm, red was generated manually).

3 Results

Minimization of Residual Stress In Fig. 4 we sketch typical calibration curves showing change in pixel-averaged intensity (ΔI_0) as a function of applied force. For spheres which we incubated at elevated temperatures to remove residual stress (red dash dot curve), we observed a monotonic dependence on applied force, which is ideal for force measurement applications. On the other hand, if care is not taken to remove residual stress, then at zero applied force the spheres have an appreciable photoelastic signal. Depending on the amount of residual stress, this can lead to reduced ΔI_0 for the same applied force (green dashed curve), or even non-monotonic dependence of ΔI_0 on applied force (blue solid curve). Clearly, a non-monotonic dependence on applied force is not suitable for force measurement, but reduced intensity changes also decrease the potential accuracy of force measurements, since intensity measurements would not discriminate as strongly between different amounts of force. Thus, we found that minimization of residual stress is key to fabricating spheres for photoelastic force measurement. In the following, we call the slope of a linear fit to the calibration curve the sensitiv-

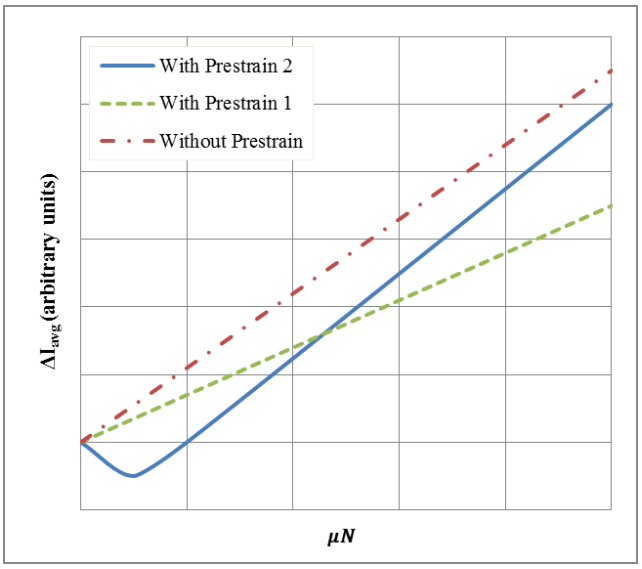

Fig. 4 Schematic of typical calibration curves of changes in pixel-averaged intensity as a function of applied force for different conditions of prestrain.

ity and use it as a measure of the force-discrimination ability of our photoelastic spheres.

Effect of Salt Concentration The spheres were stored and annealed in NaCl solutions with concentrations varying from 0 M to 1 M. Figure 5a) shows results for 12% gelatin spheres stored in different salt concentration. Different salt concentrations have different slopes and hence sensitivities; we plot the sensitivity as a function of salt concentration from 0.164 M to 1 M in Fig. 5(b). The sensitivity increases with increasing salt concentration; however, we emphasize that our spheres show photoelastic capabilities across our entire range of concentrations. Therefore, the spheres can be used with a wide variety of organisms living in different saline environments, from freshwater to marine sands with 0.6 M concentration. In the rest of the paper, we choose a single intermediate salt concentration of 0.33M NaCl to investigate in more detail the photoelastic properties of the spheres.

Effect of Gelatin Concentration Calibration curves for different gelatin concentration stored in 0.33M salt concentration are shown in Fig. 6a. The resulting sensitivities as a function of gelatin concentration are shown in Fig. 6b. 14% gelatin concentration has the lowest sensitivity, while lower concentrations do not show strong dependence on gelatin concentration. While sensitivity does not favor one gelatin concentration over others, the structural integrity (i.e., ability to withstand force without permanent deformation) of the spheres

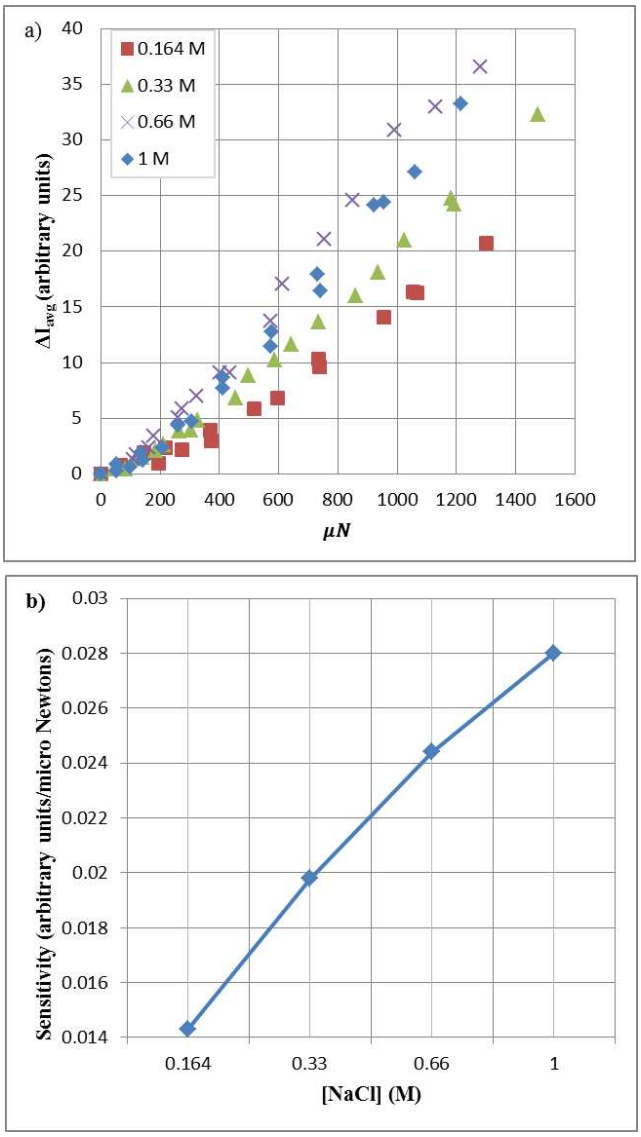

Fig. 5 (a)Changes in pixel-averaged intensity as a function of applied force and b)corresponding sensitivities for 12% gelatin spheres stored in variable NaCl solutions.

also varies with gelatin concentration and can be important if one needs to measure forces greater than 1000 μN. For instance, 6% gelatin spheres usually can bear forces around 1300 μN, but they show permanent deformation at higher forces. In contrast, 12% gelatin can easily bear forces greater than the maximum calibration force we applied (8000 μN) without permanent deformation. Finally, we also observed that 12% gelatin spheres had more consistent properties than 6% gelatin spheres or 8% gelatin spheres.

Therefore, for many applications 10-12% gelatin spheres have an appropriate combination of good sensitivity and structural integrity. However, based on the tradeoffs between the three effects discussed above, other gelatin concentrations may be more optimal. For exam-

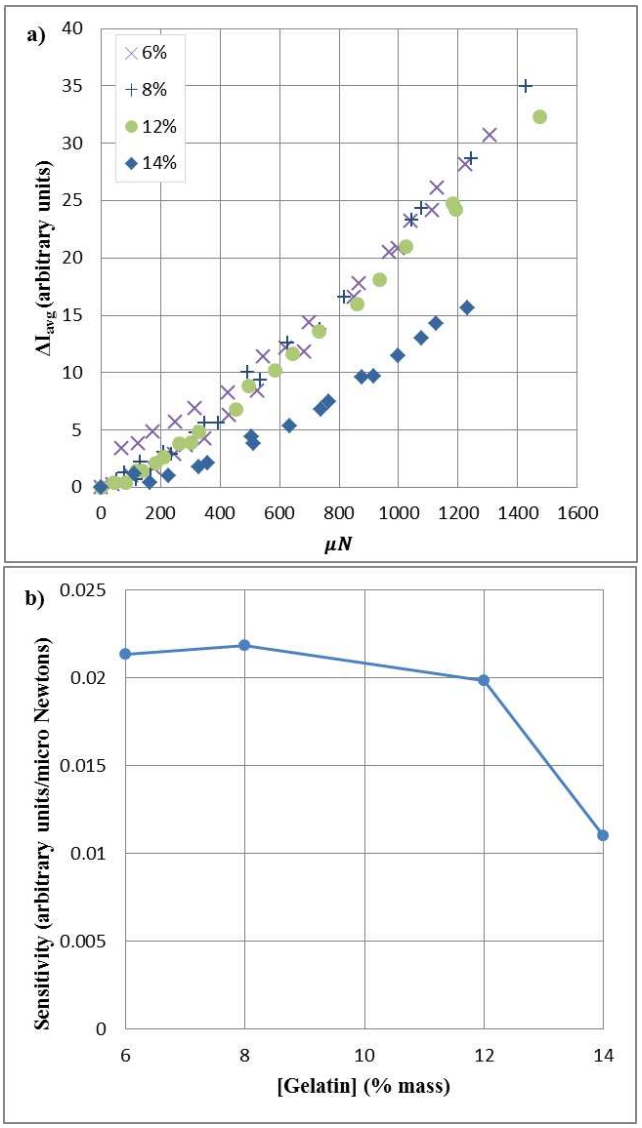

Fig. 6 (a) Changes in pixel-averaged intensity as a function of applied force and b) corresponding sensitivity for variable gelatin concentration spheres stored in 0.33M NaCl solution.

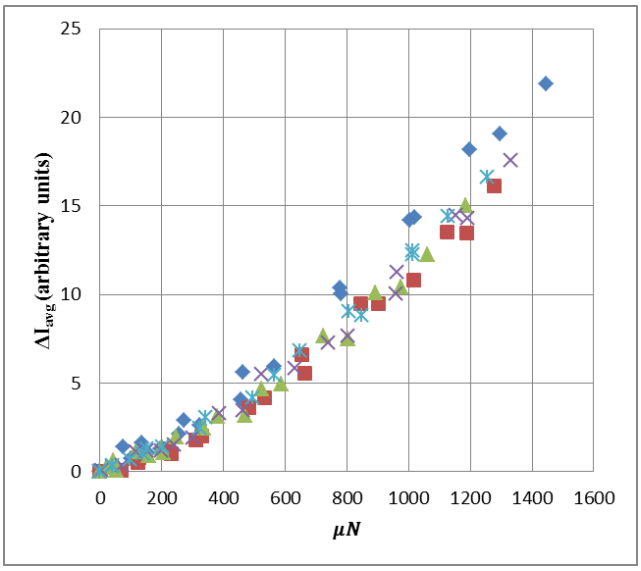

Fig. 7 Changes in pixel-averaged intensity for five consecutive loading-unloading cycles. The tested sphere contains 12% gelatin mass concentration stored in 0.33M NaCl solution.

ple, if structural integrity is more important and only large-magnitude forces are of interest, higher gelatin concentrations may be more appropriate.

Repeatability of Photoelastic Response In experiments with burrowing organisms, a sphere may be loaded and unloaded multiple times by an organism. Therefore, we examined how a single sphere responds to repeated cycles of compression and decompression. In Fig. 7 we show signal vs force measurements for 5 compression-decompression cycles on the same 12% gelatin sphere stored in 0.33 M NaCl solution. We did not observe significant hysteresis for compression and decompression; the results from each cycle are consistent. This behavior confirms that the gelatin spheres have consistent calibration curves across time as they are loaded and unloaded multiple times by a burrowing organism.

In situations where a granular material composed of many spheres is subjected to forces exerted by organisms, it would be impractical to measure the calibration curve of every single sphere. Instead, it is more feasible to measure calibration curves for a sample of spheres and use the results for all the spheres. For this to be applicable, the calibration curves must be repeatable and consistentfor different spheres. We examined repeatibility in two ways. First, we examined the variation in calibration curves for different spheres taken from a single fabrication process. Second, we examined the variation in calibration curves for spheres taken from different fabrications using the same nominal gelatin and salt concentration.

In Fig. 8 we show calibration curves for 5 different spheres fabricated from the same 12% gelatin solution and stored in 0.33 M NaCl solution. The results from each sphere are broadly consistent with the others although there is variation. For example, the force applied to create an average ΔI_0 of 10 (arbitrary units) ranges from 691μN to 903μN. In Fig. 9 we show calibration curves for 10 spheres, each fabricated on a different day using fresh 12% gelatin solution and stored in 0.33 M NaCl solution. Again, the calibration curves were consistent between batches with some variation. For example, the force applied to create an average signal change of 10 arbitrary units ranges from 397μN to 598μN. In the next section we describe the effect of the variation o nforce quantification.

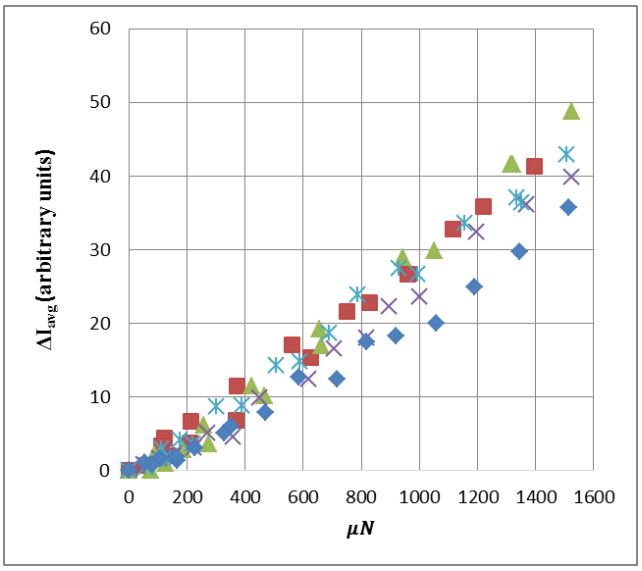

Fig. 8 Changes in pixel-averaged intensity as a function of applied force for five 12% gelatin mass concentration stored in 0.33M NaCl solution. The tested spheres were selected randomly from one batch of fabricated spheres.

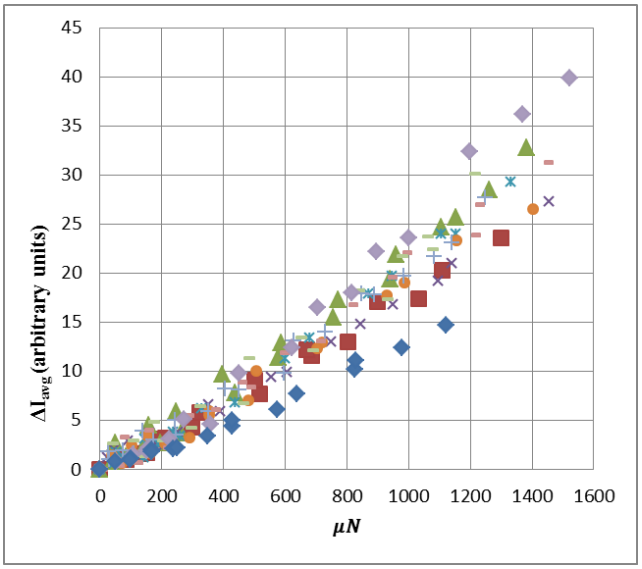

Fig. 9 Changes in pixel-averaged intensity as a function of applied force for ten 12% gelatin mass concentration stored in 0.33M NaCl solution. The tested spheres were selected randomly from different batches of fabricated spheres.

Quantitative Force Measurement From Calibration Curves The purpose of the calibration curves is to allow image analysis of photoelastic signal from gelatin spheres to deduce the force applied to the spheres in the context of burrowing in granular motion. Here we analyze force detection limits and the precision of forces deduced from our calibration curves. In this scenario, the measured variable is the change in photoelastic signal and the deduced variable is the applied force, so we replot the data from Figs. 8 and 9 with the signal on the horizontal axis and the force on the vertical axis. To provide the force and error corresponding to an observed change in pixel-averaged intensity ΔI_0, we assume that the mean applied force $\bar{f}$ resulting in signal ΔI_0 takes a quadratic form

$$\bar{f}(\Delta I_0) = A\Delta I_0 + B\Delta I_0^2 \tag{2}$$

and for value of ΔI_0 the corresponding forces take a normal distribution with standard deviation

$$\sigma(\Delta I_0) = C + D\Delta I_0 + E\Delta I_0^2. \tag{3}$$

We performed a maximum likelihood estimate of the parameters A, B, C, D, and E using the data in Figs. 8 and 9. If the data points are $(\Delta I_o^i, f^i)$, we maximized the logarithm of the likelihood function $P(A, B, C, D, E) = \prod_i p^i$ with respect to A, B, C, D, and E, where

$$p^i = \frac{1}{\sigma(\Delta I_0^i)\sqrt{2\pi}} \exp\left[\frac{-1}{2\sigma(\Delta I_0^i)^2}(\bar{f}(\Delta I_0^i) - f^i)^2\right]. \tag{4}$$

Within the same batch (Fig. 8), we found that $A = 49.2400$, $B = -0.3790$, $C = 59.8103$, $D = 1.7464$, and $E = 0.0127$. This yielded the calibration curve in Fig. 10a for force as a function of signal (red solid line), with the black dashed lines showing one standard deviation from the mean force at each signal. Across different batches (Fig. 9), $A = 63.9948$, $B = -0.6894$, $C = 62.7330$, $D = 1.8374$, and $E = 0.0135$, with the corresponding calibration curve and error in Fig. 11. Note that for each curve, 83 data points are used to fit the 5 model parameters in Fig. 10 and 178 data points are used to fit the 5 model parameters in Fig. 11. The results shown in Fig. 10 and 11 show *a posteriori* that the model reasonably represents the data.

The error $\sigma(\Delta I_0)$ for both cases are also plotted separately in Fig. 10b. The standard deviation for the same batch and different batch are shown in 12. The results for different batches have greater standard deviation than the same batch. Based on these results, for best performance, each batch should be calibrated independently before use.

We note that the error estimates are based upon the assumed quadratic form in Eq. 3, and need to be interpreted carefully for the lowest signal strengths. In particular, negative forces cannot produce any photoelastic signal. We observed that for any given sphere we could consistently detect a change in pixel-averaged intensity for $1\,\mu$N forces, which is the smallest force that our balance can resolve. However, the calculated error near zero signal was about 60μN. Therefore, if $\bar{f}(\Delta I_0) < \sigma(\Delta I_0)$, the quantitative force range corresponding to the signal ΔI_0 should be $[0, \bar{f} + \sigma]$ rather than $[\bar{f} - \sigma, \bar{f} + \sigma]$. Furthermore, our observations imply that the minimum force detection threshold for our

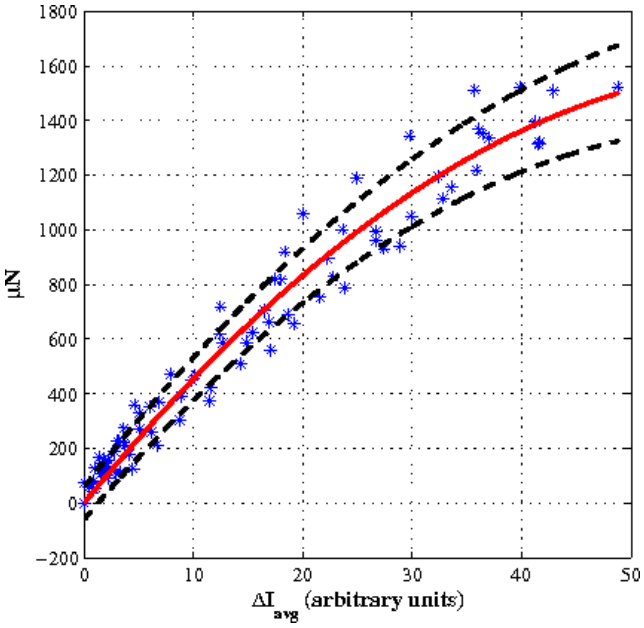

Fig. 10 Calibration curve for changes in pixel-averaged intensity as a function of applied force for five 12% gelatin mass concentration stored in 0.33M NaCl solution selected randomly from the same batch (red line, mean; black dash lines, ± standard deviation). As described in the text, the calibration curve and standard deviation are obtained based on a maximum-likelihood estimation.

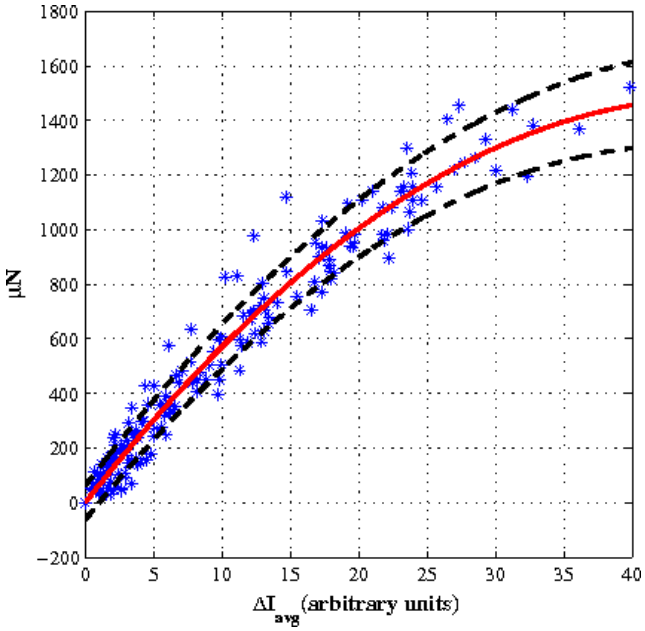

Fig. 11 Calibration curve for changes in pixel-averaged intensity as a function of applied force for ten 12% gelatin mass concentration spheres stored in 0.33M NaCl solution selected randomly from variable batches (red line, mean; black dash lines, ± standard deviation). As described in the text, the calibration curve and standard deviation are obtained based on a maximum-likelihood estimation.

technique is $< 1\mu$N, which is limited by the sensitivity of our scale. This suggests that quantitative force analysis could be improved if more consistent fabrication of gelatin spheres could be achieved, for example by carefully controlling the size and spherical shape of the beads.

Application to Animal Locomotion in Granular Media We provide a proof-of-principle in which we visualized the force distribution in a granular media as the earthworm *L. terrestis* burrowed through it. Here, the purpose is only to validate the applicability and biocompatibility of our gelatin spheres with a live organism; earthworms typically burrow through cohesive soils rather than the noncohesive granular medium made using our gelatin spheres. Nonetheless, in extremely waterlogged environments earthworms may encounter noncohesive substrates that must be navigated.

In this experiment (Fig. 13), we separated two glass plates by 6.13 mm using a plastic ring. The ring was glued to the bottom plate, so that it could be filled with waterand gelatin spheres of diameter about 3 mm. A worm was then added to the water and gelatin, and the entire assembly was imaged in the polariscope (oriented so that the plates were horizontal). We placed the worm in 0.33 M NaCl solution to induce activity. The worms were removed from the salt solution after

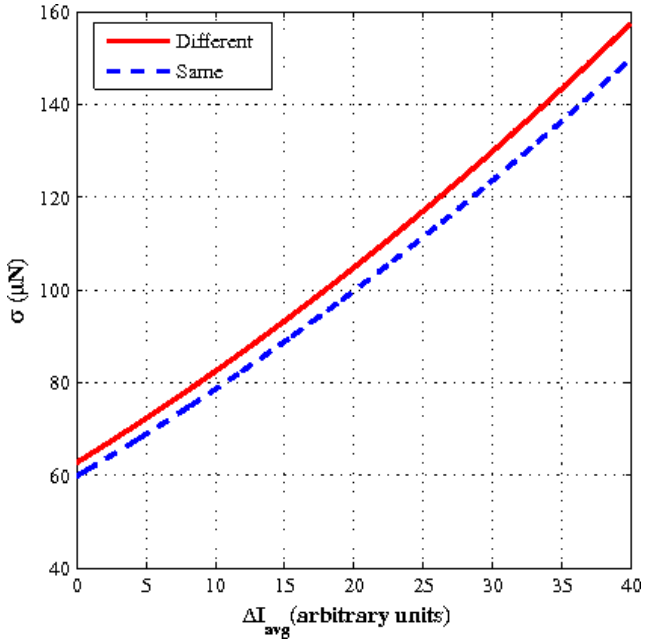

Fig. 12 Calculated error of applied force as a function of changes in pixel-averaged intensity. The solid red line and dashed blue line show the error in deduced applied force for spheres randomly selected from different batches and the same batch, respectively. As described in the text, the calibration curve and standard deviation are obtained based on a maximum-likelihood estimation.

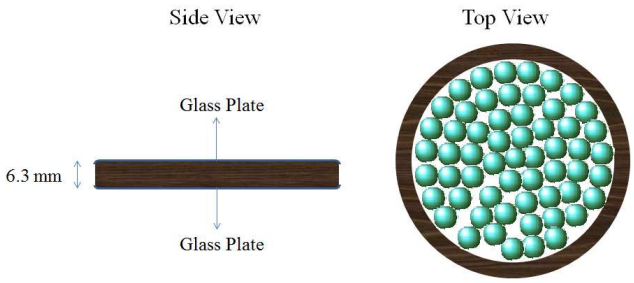

Fig. 13 Schematic of granular medium setup. The sample glass container is filled with NaCl solution and gelatin spheres. Then a glass lid is located over the container.

10 minutes and rinsed with fresh water before returning them to soil. In the granular material, the worm seemed to make similar movements as observed during burrowing in cohesive soils[17, 16]. As Fig. 14 and the video (Online Resource 1) show, these spheres can resolve the forces exerted during locomotion of the earth worm. Networks of force chains can be seen as the illuminated lines of gelatin spheres.

We quantified the force exerted by the worm at selected spheres in one image (Fig. 14). First we calibrated five spheres randomly selected from the container following the procedures discussed earlier. We used as a reference image an image of the granular medium without the worm. Then the worm was added to this media and the spheres imaged during locomotion. From the images, the boundaries of the spheres were identified by first locating contact points (where the photoelastic signal is most intense), then fitting circles that intersect the contact points. In this experiment we did not compare the signal of each sphere to a reference image of the same sphere, because spatial variation in our light source lead to differences in reference intensity at different locations. Instead, we compared the intensity of a sphere to the intensity of a reference sphere in the same position in the reference image. This method of referencing leads to an additional error since different spheres have different zero-force intensities. To estimate this error we selected five gelatin sphere and found the standard deviation in their pixel-averaged intensity with zero applied force. We added this error in quadrature to the error obtained from the maximum likelihood estimate of errors in our calibration.

Figure 14 shows a worm which was extending one end near the middle of the container rightwards. We measured the forces exerted by the worm as it rearranges the spheres during this extension at five locations. In this image, it was difficult to determine the boundaries of spheres very close to the extending portion of the worm, so we selected spheres in force chains caused by the extension a few spheres away from the

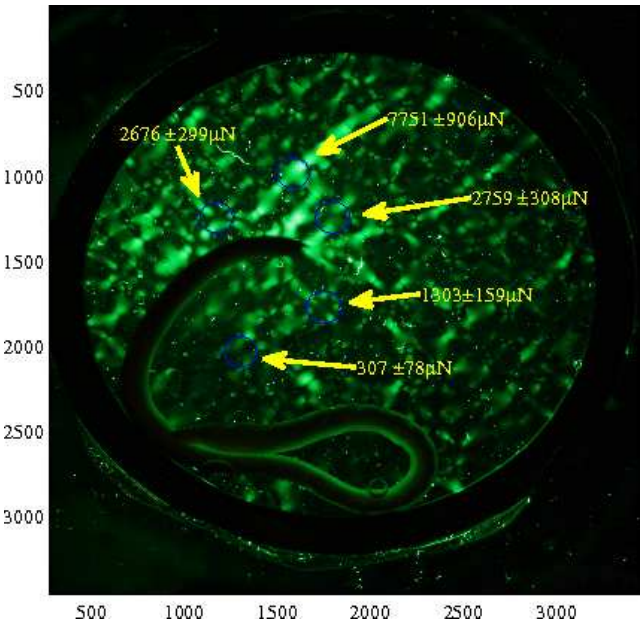

Fig. 14 Proof-of-principle experiment with a worm moving through a layer of photoelastic gelatin spheres. Networks of force chains are seen as the illuminated lines of gelatin spheres. Five sample spheres were selected to show forces.

worm. The earthworm generates forces in the range from 300μN to 8 mN during this extension. These values of forces are significantly smaller than those exerted during burrowing through cohesive soils, likely due to the fact that our noncohesive medium requires much smaller forces to rearrange. Note that the most sensitive photoelastic disk experiments for granular media we know of reported sensitivities in the mN range[5]. At mN sensitivity, plastic disks would only be able to detect the largest of the forces we measured, but our spheres are sensitive enough to quantify the entire range of forces exerted by the worm on this medium. Correlation of the visualized force patterns and worm kinematics is left for future work and will require video image analysis to automatically track multiple spheres and worm body kinematics.

4 Discussion

We developed a new method of manufacturing large quantities of gelatin spheres with adequate photoelastic properties. These spheres are more flexible in application and more photoelastically sensitive than conventional photoelastic disks making them suitable for use with organisms. A high precision calibration method was developed and sources of error were greatly reduced or controlled. A storage method was developed that allowed control of gelatin hydration, residual stress and long-term storage of spheres. We discussed how the

gelatin concentration and salt concentration used during sphere fabrication and storage may be selected to make the spheres compatible to use with a wide range of organisms. Based on the repeatibility of the calibration curves, we found that each batch of spheres fabricated should be calibrated separately by sampling a population of the batch. Finally, as a proof-of-principle, we showed that our system can be used to quantify force exerted by an earthworm.

After minimizing residual stress, we consistently detected photoelastic signal for forces at the 1μN sensitivity limit of our force-measuring scale. The current quantitative precision of our photoelastic system is around $60\,\mu$N for the smallest forces, varying up to 150 μN for forces of around 1450 μN. This is a two order of magnitude improvement on previously reported force sensitivities using photoelastic disks, and is sufficient to resolve the forces of all but the smallest worms such as *C. elegans*. The flexibility in creating spheres of different sizes also opens up possibilities to simulate a variety of different noncohesive soil types and environments.

What are the prospects for extending the use of gelatin spheres to an organism such as *C. elegans*? Previous investigations of *C. elegans* in granular media used beads of diamter $\sim 100\,\mu$m[11, 12]. To answer this question, we investigated how photoelastic method depended on sphere size. The sizes we fabricated ranged from less than 100 μm to about 7 mm, but our calibration equipment could only clearly visualize spheres greater than about 1 mm. Several conveniently sized spheres were chosen for testing (Fig. 15(a)). (Fig. 15(b)) shows the sensitivity of gelatin spheres for different sizes, which shows that for this small range of sizes, the sensitivity tends to increase as the size is decreased.

We can also use scaling arguments to estimate how the sensitivity should scale with sphere size: Photoelastic signal intensity decreases linearly with path length and increases linearly with stress. Smaller sphere diameters have smaller cross sections, meaning a higher strain for the same load, but a shorter path length. Path length is linearly related to sphere diameter and stress is inversely related to the diameter squared, so we expect that intensity for the same load, and hence sensitivity and precision, is inversely related to sphere diameter. Based on this scaling argument and our experiments with 1 mm-scale spheres, for $\sim 100\mu$m diameter spheres which are a factor of ten smaller than 1 mm spheres, the minimum detection threshold would be ten times smaller than our current $1\,\mu$N detection threshold, or $\sim$ 100nN, and the precision for force measurements would be $\sim 6\,\mu$N. This threshold provides detection within the range of approximately $< 1\,\mu$N forces reported for *C. elegans* using other measurement techniques [7, 18], but accurate quantification of the forces exerted by *C. elegans* would require more consistent fabrication of gelatin spheres than what we have achieved so far.

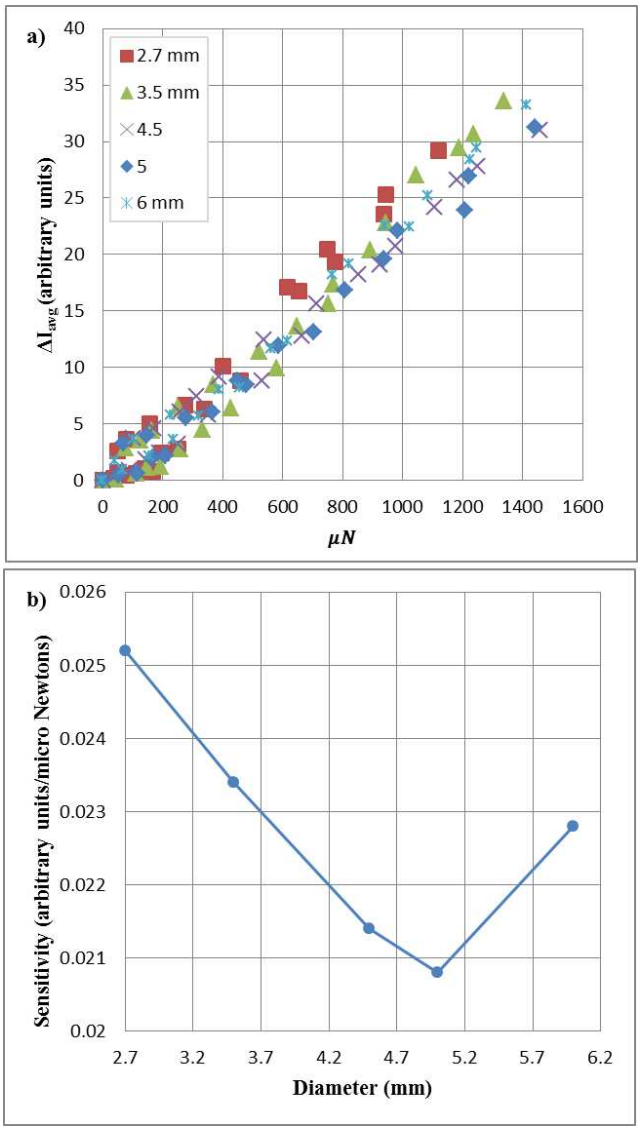

Fig. 15 (a)Changes in pixel-averaged intensity as a function of applied force and b)correspodning sensitivity for gelatin spheres with six different sizes. Gelatin spheres with 12% mass concentration stored in 0.33M NaCl solution were selected for the test.

Finally, our spheres may be useful for applications outside of granular locomotion, since they provide a way to accurately measure small forces in appropriate environments. For example, they may be useful for sensing local pressures or in investigations of weak adhesion forces.

Acknowledgements We thank Abe Clark for information about photoelastic disks. HCF, AM, and MJ were supported

by National Science Foundation award CBET-1252182-CAREER to HCF.

References

1. Che J, Dorgan KM (2010) Its tough to be small: dependence of burrowing kinematics on body size. Journal of Experimental Biology 213:1241–1250
2. Doll J, Harjee N, Klejwa N, Kwon R, Coulthard S, Petzold B, Goodman M, Pruitt B (2009) SU-8 force sensing pillar arrays for biological measurements. Lab on a chip 9:1449–1454
3. Dorgan KM, Arwade S, Jumars P (2007) Burrowing in marine muds by crack propagation: kinematics and forces. The Journal of Experimental Biology 210:4198–4212
4. Dorgan KM, Law CJ, Rouse GW (2013) Meandering worms: mechanics of undulatory burrowing in muds. Proc R Soc B 280(1757):20122,948
5. Estep J, Dufek J (2012) Substrate effects from force chain dynamics in dense granular flows. Journal of Geophysical Research-Earth Surface 117:F01,028
6. Full RJ, Yamauchi A, Jindrich D (1995) Maximum single leg force production: cockroaches righting on photoelastic gelatin. Journal of Experimental Biology 198:2441–2452
7. Ghanbari A, Nock V, Wang W, Blaikie R, Chase G, Chen X, Hann CE (2008) Force pattern characterization of *C. elegans* in motion. In: Proceedings of 15th International Conference on Mechatronics and Machine Vision in Practice, pp 680–685
8. Harris JK (1978) A photoelastic substrate technique for dynamic measurements of forces exerted by moving organisms. Journal of Microscopy 114(2):219–228
9. Herrel A, Choi HF, Dumont E, Schepper ND, Vanhooydonck B, Aerts P, Adriaens D (2011) Burrowing and subsurface locomotion in anguilliform fish: behavioral specializations and mechanical constraints. Journal of Experimental Biology 214:1379–1385
10. Jessop HT, Harris FC (1960) Photoelasticity, Principles and Methods. Dover Publications, New York
11. Juarez G, Lu K, Sznitman J, Arratia PE (2010) Motility of small nematodes in wet granular media. EPL (Europhysics Letters) 92:44,002
12. Jung S (2010) *Caenorhabditis elegans* swimming in a saturated particulate system. Physics of Fluids 22:031,903
13. Majmudar TS, Behringer RP (2005) Contact force measurements and stress-induced anisotropy in granular materials. Nature, 435:1079–1082
14. Maladen RD, Ding Y, Li C, Goldman DI (2009) Undulatory swimming in sand: Subsurface locomotion of the sandfish lizard. Science 325:314–318
15. Murphy EAK, Dorgan KM (2011) Burrow extension with a proboscis: mechanics of burrowing by the glycerid *Hemipodus simplex*. The Journal of Experimental Biology 214:1017–1027
16. Quillin K (1999) Kinematic scaling of locomotion by hydrostatic animals: ontogeny of peristaltic crawling by the earthworm *Lumbricus terrestris*. The Journal of Experimental Biology 202:661674
17. Quillin K (2000) Ontogenetic scaling of burrowing forces in the earthworm *Lumbricus terrestris*. The Journal of Experimental Biology 203:2757–2770
18. Shen XN, Sznitman J, Krajacic P, Lamitina T, Arratia PE (2012) Undulatory locomotion of *C. elegans* on wet surfaces. Biophysical Journal 102:27722781
19. Wendell DM, Luginbuhl K, Guerrero J, Hosoi A (2012) Experimental investigation of plant root growth through granular substrates. Experimental Mechanics 52(7):945–949
20. Winter AG, Deits VRLH, Hosoi AE (2012) Localized fluidization burrowing mechanics of *Ensis directus*. Journal of Experimental Biology 215:2072–2080